Science Advances

AAAS

advances.sciencemag.org/cgi/content/full/3/12/eaap7528/DC1

Supplementary Materials for

Induced seismicity provides insight into why earthquake ruptures stop

Martin Galis, Jean Paul Ampuero, P. Martin Mai, Frédéric Cappa

Published 20 December 2017, *Sci. Adv.* **3**, eaap7528 (2017)
DOI: 10.1126/sciadv.aap7528

This PDF file includes:

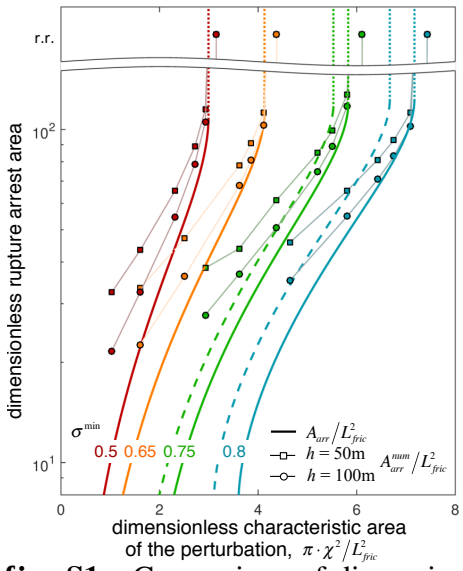

fig. S1. Comparison of dimensionless rupture arrest area calculated from numerical simulations with grid spacing $h = 50$ m (circles) and $h = 100$ m (squares) with our theoretical estimates (bold lines) for varying σ^{min} (indicated by color). To facilitate the comparison, theoretical curves for $\sigma^{min} = 0.75$ and 0.8 were shifted to match the transition to runaway ruptures for numerical results (the original position is depicted by bold dashed lines). The comparison reveals that finer grid sampling leads to better agreement between numerical simulations and our theoretical estimates. $L_{fric} = \mu \cdot D_c/(\tau_{s0} - \tau_{d0})$ is a characteristic length scale introduced by the slip-weakening process (*39*).

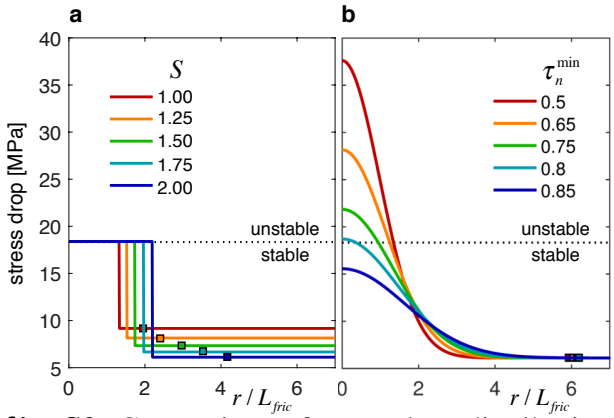

fig. S2. Comparison of stress drop distributions as functions of dimensionless crack radius at the time of A_{arr}^{max} for situations from Fig. *6*. a) for a step-like distribution of stress drop with varying strength parameter S b) for a Gaussian distribution of stress drop with varying normal stress. Filled symbols indicate R_{max}. $L_{fric} = \mu \cdot D_c/(\tau_{s0} - \tau_{d0})$ is a characteristic length scale introduced by the slip-weakening process (*39*).

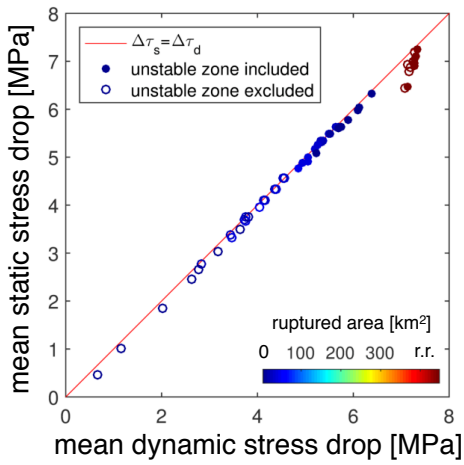

fig. S3. Scaling of mean static and dynamic stress drops in results of numerical simulations. Ruptured area (color-coded) indicate that our assumption ($\delta\tau_s = \delta\tau_d$) is valid for arrested ruptures (shades of blue). The runaway ruptures (dark red) in numerical simulations have to be eventually arrested by an artificial barrier, which leads to deviations from the ideal scaling, as expected (r.r. stands for runaway rupture).

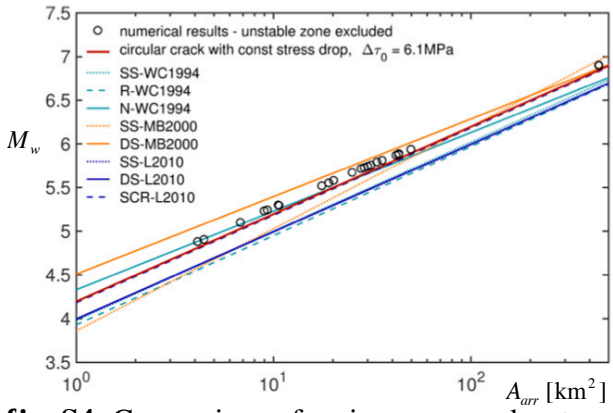

fig. S4. Comparison of various approaches to estimate M_w from ruptured area A_{arr}. Empirical scaling relations are denoted as follows: WC1994 (*40*), MB2000 (*41*), L2010 (*35*). SS stands for strike-slip, R for reverse, N for normal, DS for dip-slip events and SCR for events in stable continental regions. Note: The overlapping points for M∼7 correspond to runaway ruptures while the rest of the points correspond to arrested ruptures.

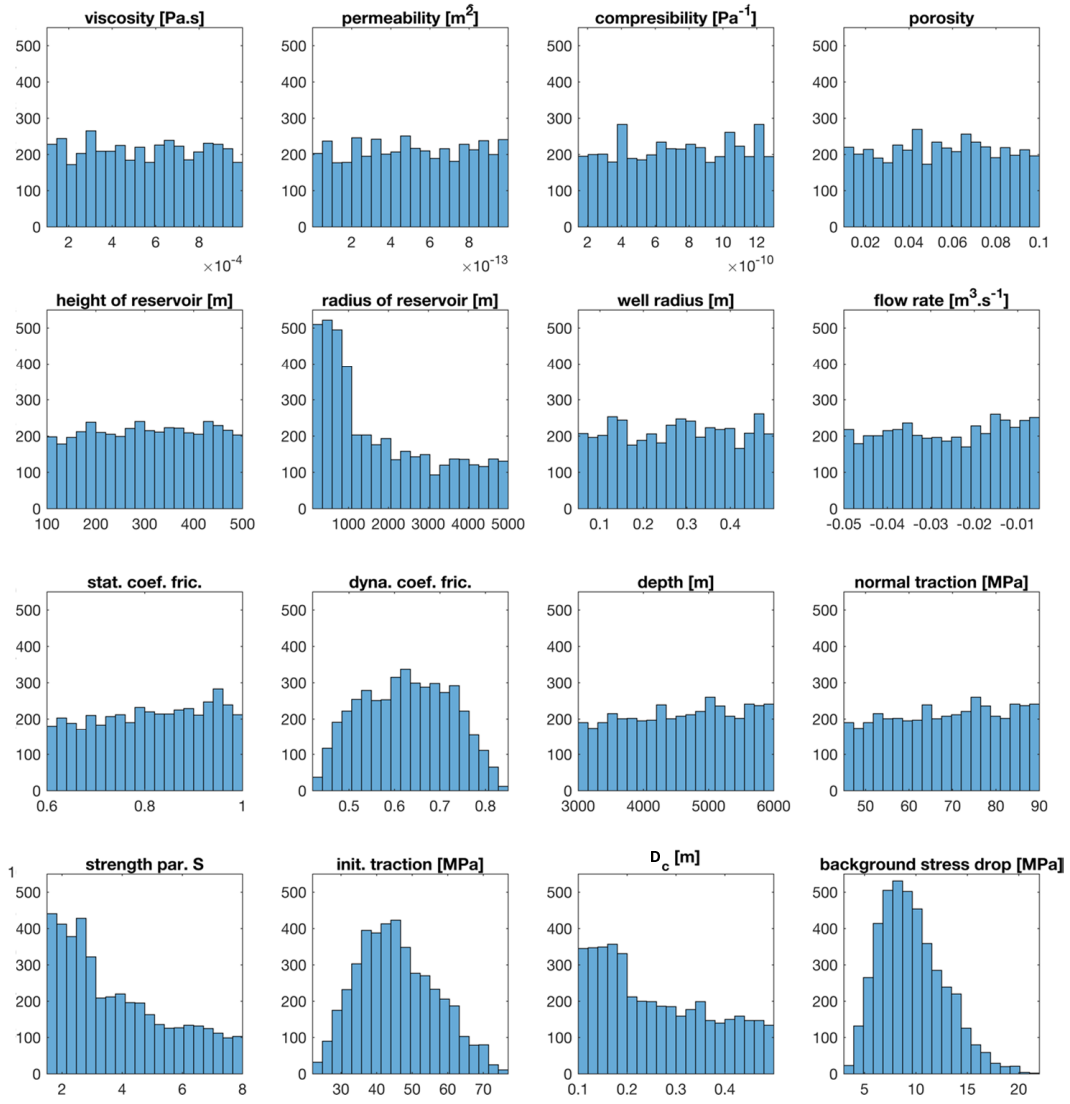

fig. S5. Distributions of reservoir-fault parameters for all ∼4250 configurations used for verification of M_w^{max} (point-load approximation) against M_w^{crit} (finite-reservoir approach). Viscosity, permeability, compressibility, porosity, height of reservoir, well radius, flow rate, static coefficient of friction, and depth of a fault were sampled from uniform probability density functions (PDFs). Radius of reservoir, strength parameter S and slip-weakening distance D_c were initially also sampled from uniform PDFs. However, to increase density of points with lower magnitudes in fig. *S7*, we increased the number of configurations presumably leading to smaller

magnitudes based on the correlations between parameters and magnitudes in fig. *S6*. Consequently, the resulting histograms are right-skewed. The remaining non-uniform distributions of dynamic coefficient of friction, initial shear stress and background stress drop are results of constraints used to compute self-consistent sets of fault-related parameters. For example, initial stress was computed such that it produces the selected S value for selected normal stress and coefficients of friction.

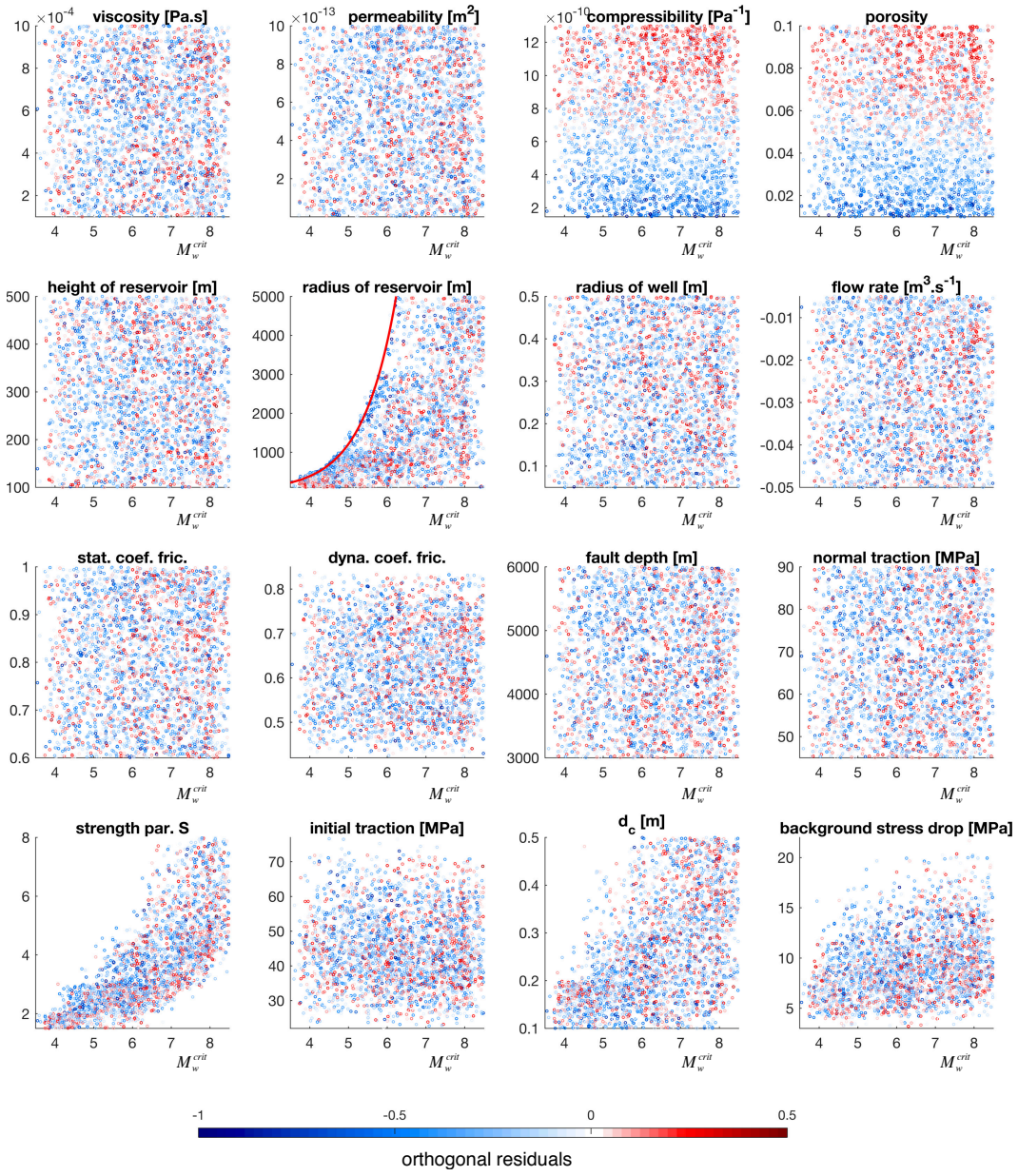

fig. S6. Distributions of reservoir-fault parameters for all ∼4250 configurations used for verification of M_w^{max} (point-load approximation) against M_w^{crit} (finite-reservoir approach). The red line in "reservoir radius" panel indicates M_w corresponding to the area of a reservoir assuming average background stress drop for all configurations. Therefore, the few points lying to the left of the line do not indicate transition to runaway rupture within a reservoir, but configurations

with higher than average stress drop. Orthogonal residuals are color-coded, revealing a weak correlation of compressibility and porosity with the residuals (this problem is further discussed in the main text). We observe correlation between parameters and magnitude only for strength parameter S, characteristic slip distance D_c and reservoir radius, for which the correlation is caused by the fact that the transition to runaway ruptures happens outside of a reservoir.

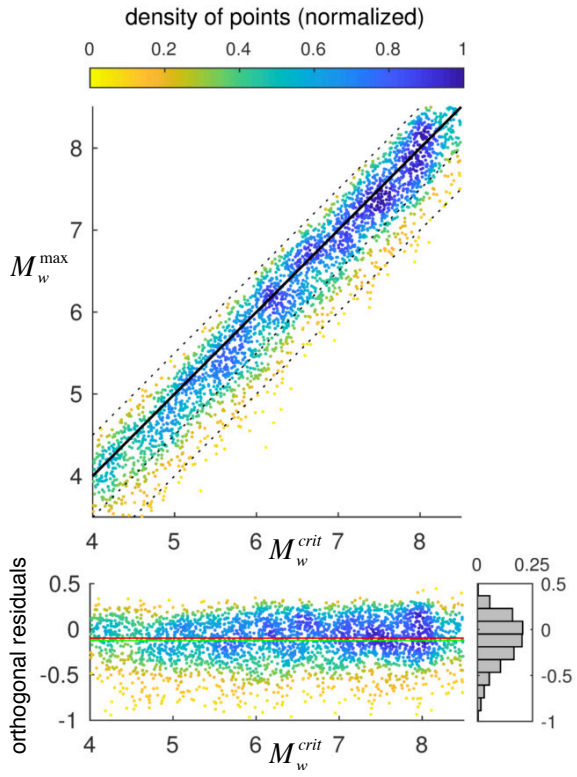

fig. S7. Comparison of $M_w^{max-arr}$ (derived for a point-load approximation of a reservoir) with M_w^{crit} (derived for a finite reservoir) and corresponding orthogonal residuals. Density of points in the plots is emphasized using a color scale. The plots reveal that $M_w^{max-arr}$ scales very well with M_w^{crit}, as indicated by residuals with mean (green) and median (red) very close to zero, although the distribution of residuals is slightly non-symmetric, as seen in the histogram.

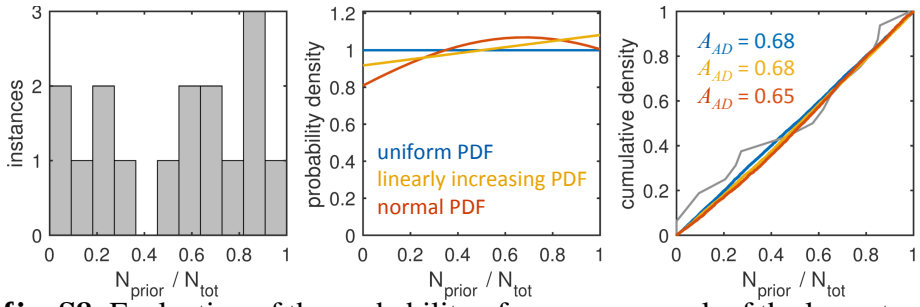

fig. S8. Evaluation of the probability of occurrence rank of the largest event within a sequence. a) Histogram of the unbiased data set by (*12*). b) Comparison of three tested probability density functions (PDFs). c) The data were tested against the three PDFs using the two-sample Anderson-Darling test (*38*). The null hypothesis - data are sampled from the corresponding PDF - is accepted if the statistic A_{AD} is lower than the critical value 2.492 (see text for further details).

table S1. Reservoir and fault parameters used to prepare Fig. *2*. Though the parameter values are chosen from intervals reported for general reservoir (*36*,*37*), they do not represent end-members. Instead, we chose parameters such that they illustrate the behavior of the system. μ_v - viscosity, k - permeability, ϕ - porosity, c_t - compressibility, h - height of reservoir, r_e - radius of reservoir, q - injection rate (negative and positive sign indicates injection or extraction, respectively), μ_d dynamic coefficient of friction, μ_s - static coefficient of friction, τ_0 - background shear stress, σ - background normal stress, D_c - characteristic slip-weakening distance, S - strength parameter, τ_{s0} - background static stress, τ_{d0} - background dynamic stress, $\Delta\tau_0$ - stress drop, $\Delta\tau_E$ - strength excess. The gray values are identical with the reference case.

	μ_v [Pa.s]	k [m²]	ϕ	c_t [Pa⁻¹]	h [m]	r_e [m]	q [m³.s⁻¹]	μ_d	μ_s	τ_0 [MPa]	σ [MPa]	D_c [m]	S	τ_{s0} [MPa]	τ_{d0} [MPa]	$\Delta\tau_0$ [MPa]	$\Delta\tau_E$ [MPa]
Fig. 2a	2.E-04	2.E-15	0.05	5.00E-10	200	1000	-0.0250	0.525	0.678	69.1	120.0	0.4	2.0	81.3	63.0	6.1	12.2
	2.E-04	2.E-15	0.05	1.45E-10	200	1000	-0.0250	0.525	0.678	69.1	120.0	0.4	2.0	81.3	63.0	6.1	12.2
	2.E-04	2.E-15	0.05	7.50E-10	200	1000	-0.0250	0.525	0.678	69.1	120.0	0.4	2.0	81.3	63.0	6.1	12.2
	2.E-04	2.E-15	0.01	5.00E-10	200	1000	-0.0250	0.525	0.678	69.1	120.0	0.4	2.0	81.3	63.0	6.1	12.2
	2.E-04	2.E-15	0.10	5.00E-10	200	1000	-0.0250	0.525	0.678	69.1	120.0	0.4	2.0	81.3	63.0	6.1	12.2
	2.E-04	1.E-15	0.05	5.00E-10	200	1000	-0.0250	0.525	0.678	69.1	120.0	0.4	2.0	81.3	63.0	6.1	12.2
	2.E-04	4.E-15	0.05	5.00E-10	200	1000	-0.0250	0.525	0.678	69.1	120.0	0.4	2.0	81.3	63.0	6.1	12.2
	1.E-04	2.E-15	0.05	5.00E-10	200	1000	-0.0250	0.525	0.678	69.1	120.0	0.4	2.0	81.3	63.0	6.1	12.2
	1.E-03	2.E-15	0.05	5.00E-10	200	1000	-0.0250	0.525	0.678	69.1	120.0	0.4	2.0	81.3	63.0	6.1	12.2
	2.E-04	2.E-15	0.05	5.00E-10	100	1000	-0.0250	0.525	0.678	69.1	120.0	0.4	2.0	81.3	63.0	6.1	12.2
	2.E-04	2.E-15	0.05	5.00E-10	500	1000	-0.0250	0.525	0.678	69.1	120.0	0.4	2.0	81.3	63.0	6.1	12.2
	2.E-04	2.E-15	0.05	5.00E-10	200	1000	-0.0075	0.525	0.678	69.1	120.0	0.4	2.0	81.3	63.0	6.1	12.2
	2.E-04	2.E-15	0.05	5.00E-10	200	1000	-0.0700	0.525	0.678	69.1	120.0	0.4	2.0	81.3	63.0	6.1	12.2
Fig. 2b	2.E-04	2.E-15	0.05	5.00E-10	200	1000	-0.0250	0.525	0.678	69.1	120.0	0.2	2.0	81.3	63.0	6.1	12.2
	2.E-04	2.E-15	0.05	5.00E-10	200	1000	-0.0250	0.525	0.678	69.1	120.0	0.8	2.0	81.3	63.0	6.1	12.2
	2.E-04	2.E-15	0.05	5.00E-10	200	1000	-0.0250	0.525	0.653	69.1	120.0	0.4	1.5	78.3	63.0	6.1	9.2
	2.E-04	2.E-15	0.05	5.00E-10	200	1000	-0.0250	0.525	0.703	69.1	120.0	0.4	2.5	84.3	63.0	6.1	15.2
	2.E-04	2.E-15	0.05	5.00E-10	200	1000	-0.0250	0.500	0.678	69.1	120.0	0.4	1.3	81.3	60.0	9.1	12.2
	2.E-04	2.E-15	0.05	5.00E-10	200	1000	-0.0250	0.545	0.678	69.1	120.0	0.4	3.3	81.3	65.4	3.7	12.2
	2.E-04	2.E-15	0.05	5.00E-10	200	1000	-0.0250	0.525	0.678	70.2	120.0	0.4	1.5	81.3	63.0	7.2	11.1
	2.E-04	2.E-15	0.05	5.00E-10	200	1000	-0.0250	0.525	0.678	68.0	120.0	0.4	2.7	81.3	63.0	5.0	13.3
	2.E-04	2.E-15	0.05	5.00E-10	200	1000	-0.0250	0.525	0.678	69.1	118.2	0.4	1.5	80.1	62.0	7.1	11.0
	2.E-04	2.E-15	0.05	5.00E-10	200	1000	-0.0250	0.525	0.678	69.1	122.0	0.4	2.7	82.7	64.0	5.1	13.6
Fig. 2c	2.E-04	2.E-15	0.05	5.00E-10	200	1000	-0.0250	0.525	0.678	72.2	120.0	0.4	1.0	81.3	63.0	9.2	9.2
	2.E-04	2.E-15	0.05	5.00E-10	200	1250	-0.0250	0.525	0.678	72.2	120.0	0.4	1.0	81.4	63.0	9.2	9.2
	2.E-04	2.E-15	0.05	5.00E-10	200	750	-0.0250	0.525	0.678	72.2	120.0	0.4	1.0	81.4	63.0	9.2	9.2
	2.E-04	2.E-15	0.05	5.00E-10	200	500	-0.0250	0.525	0.678	69.1	120.0	0.4	2.0	81.3	63.0	6.1	12.2
	2.E-04	2.E-15	0.05	5.00E-10	200	750	-0.0250	0.525	0.678	69.1	120.0	0.4	2.0	81.3	63.0	6.1	12.2
	2.E-04	2.E-15	0.05	5.00E-10	200	1250	-0.0250	0.525	0.678	69.1	120.0	0.4	2.0	81.3	63.0	6.1	12.2
	2.E-04	2.E-15	0.05	5.00E-10	200	2000	-0.0250	0.525	0.678	69.1	120.0	0.4	2.0	81.3	63.0	6.1	12.2
	2.E-04	2.E-15	0.05	5.00E-10	200	1000	-0.0250	0.525	0.678	66.7	120.0	0.4	4.0	81.3	63.0	3.7	14.7
	2.E-04	2.E-15	0.05	5.00E-10	200	1250	-0.0250	0.525	0.678	66.7	120.0	0.4	4.0	81.4	63.0	3.7	14.7